Invited paper

Optical properties of semiconductor quantum wells

MACIEJ BUGAJSKI, KAZIMIERZ REGIŃSKI
Institute of Electron Technology, Warsaw, Poland

In this article we review the optical properties of semiconductor quantum wells. Special attention is paid to the phenomena involving excitons in quantum wells. We discuss both two-particle excitons in undoped quantum wells as well as many body Coulomb effects (collective excitons) in quantum wells containing high density charge carriers. We illustrate the material with our own results from recently published works on exciton dynamics and Fermi-edge singularity in modulation doped quantum wells.

First, we report high-resolution, picosecond laser spectroscopy measurements of relaxation of lowest-energy heavy-hole excitons in undoped GaAs quantum wells grown with and without growth interruptions. In both cases excitons relax by loosing potential energy in a diffusion motion driven by potential fluctuations in the quantum well plane. We have also studied directly, intrinsic properties of excitons in quantum wells, i.e., we have determined the lifetime of $k = 0$ excitons, which is a fundamental parameter of the system and has been assessed by many theories.

Then we report results of the study of many-body correlation enhancement in excitonic luminescence in dense one-component plasma. The dynamic response of an electron Fermi sea to the presence of optically generated holes gives rise to an enhanced interaction of correlated electron-hole pairs near the Fermi level, resulting in an enhanced oscillator strength for optical transitions, referred to as the Fermi-edge singularity (FES). We have studied this effect in modulation-doped quantum wells which provide confined dense Fermi sea, spatially separated from dopant atoms, easily accessible for investigations under low excitation conditions. The FES has been observed in both photoluminescence (PL) and photoluminescence excitation (PLE) experiments, although in the case of PL the samples had to be either co-doped with acceptors in the wells to provide necessary localization of holes or designed to allow for nearly resonant scattering between the electronic states near the Fermi energy and the next unoccupied subband of the 2D electron gas. The presented results are of interest from the fundamental point of view. Such effects are also important for the modelling of optoelectronic device operation under high injection conditions.

* corresponding author: Maciej Bugajski, Institute of Electron Technology, Al. Lotników 32/46, 02-668 Warsaw, Poland.

1. Introduction

The development of sophisticated growth techniques for layered semiconductor structures has initiated a large body of new work in semiconductor physics over the last twenty years. Much of the interest was stimulated by possibility of application of low dimensional structures in semiconductor lasers and related optoelectronic technology in communications and consumer products. The commercial success of quantum well lasers have furthermore created a need for in depth understanding of optical properties of these structures. This paper reviews the physics of optical properties of quantum wells pertinent to the operation of optoelectronic devices. The excitons in low dimensional structures are treated in considerable details because of their importance in quantum confined systems.

We start with a summary of basic linear optical properties of quantum wells (Section 2) and exciton dynamics in quantum wells will be discussed in Section 3. In the Section 4 we will go beyond a one-electron picture considering consequences of screening in electron-hole plasma on the optical transitions in systems of reduced dimensionality. The role of screening will be analyzed in particular in one-component plasmas where its most important consequence is the Fermi-edge singularity. We will concentrate throughout the article mainly on our recently published results in this field [1–9] which means that the review given will be somewhat selective and limited to the area of our interest. The readers interested in a broader perspective are referred to the excellent review articles [10–12]. We will not treat here optical properties of quantum wells embedded in microcavities. This is rapidly growing area of research which deserves a separate treatment. A good introduction to the subject might be found in [13].

2. Linear optical properties of quantum wells

Excitons are the quasi-particles of the lowest electronic excitations in intrinsic semiconductors. The Coulomb attraction between an electron and a hole leads to a hydrogen-like resonance below the band-gap energy and a Sommerfeld enhancement of the band-to-band transitions.

$$E_n^{3D} = E_g - \frac{Ry^*}{n^2} + \frac{\hbar^2 (K_x^2 + K_y^2 + K_z^2)}{2M} \quad (1)$$

with:

$n = 1, 2, 3,...$ principal quantum number

$Ry^* = 13.6\text{eV} \frac{\mu}{m_0} \frac{1}{\varepsilon^2}$ exciton binding energy

$M = m_e + m_h$, $\mathbf{K} = \mathbf{k}_e + \mathbf{k}_h$ translational mass and wave vector of the exciton

$\mu = \frac{m_e m_h}{m_e + m_h} m_0$ reduced mass

We use a capital **K** for the exciton wave vector to distinguish two-particle states from one-particle states. Using the material parameters for typical semiconductors one finds that excitonic Rydberg is of the order of a few meV to a few tens of meV, which is considerably less than the width of the forbidden gap. The orbits of the electron and hole around their center of mass average over many unit cells which in turn justifies the effective mass approximation used for the description of excitons in semiconductors. For $n \to \infty$ exciton states converge to the ionization continuum, the onset of which coincides with E_g.

The confinement of the carriers in quantum wells leads to the quantization of the eigenenergies in the direction perpendicular to the layers and a parabolic dispersion due to the free in plane motion (Fig.1). The in-plane dispersion is rather complicated. The degeneracy of the heavy-hole (hh) and the light-hole (lh) valence bands is removed due to the reduced translational symmetry. Besides that, the bands are strongly mixed and anticross somewhere in the Brillouin zone. The carrier confinement in quantum wells strongly modifies the properties of 2D excitons comparing to their bulk counterparts. The Schrödinger equation for the exciton problem can be solved for the exact two-dimensional case [14]. The eigenenergies of the exciton Hamiltonian:

$$E_n^{2D} = E_g + E_{nz,e} + E_{nz,h} - \frac{Ry^*}{(n - 1/2)^2} + \frac{\hbar^2 (K_x^2 + K_y^2)}{2M} \quad (2)$$

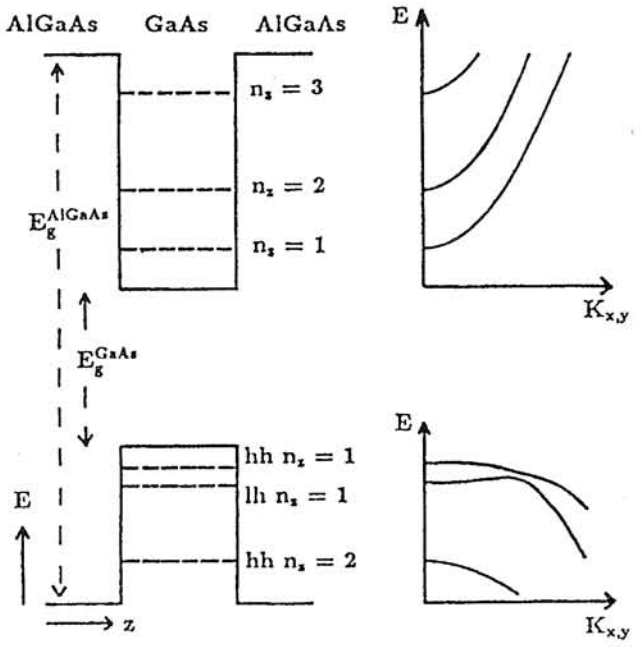

Fig.1. Confined electron and hole energy levels and subband dispersion in the x-y plane for a GaAs/AlGaAs quantum well.

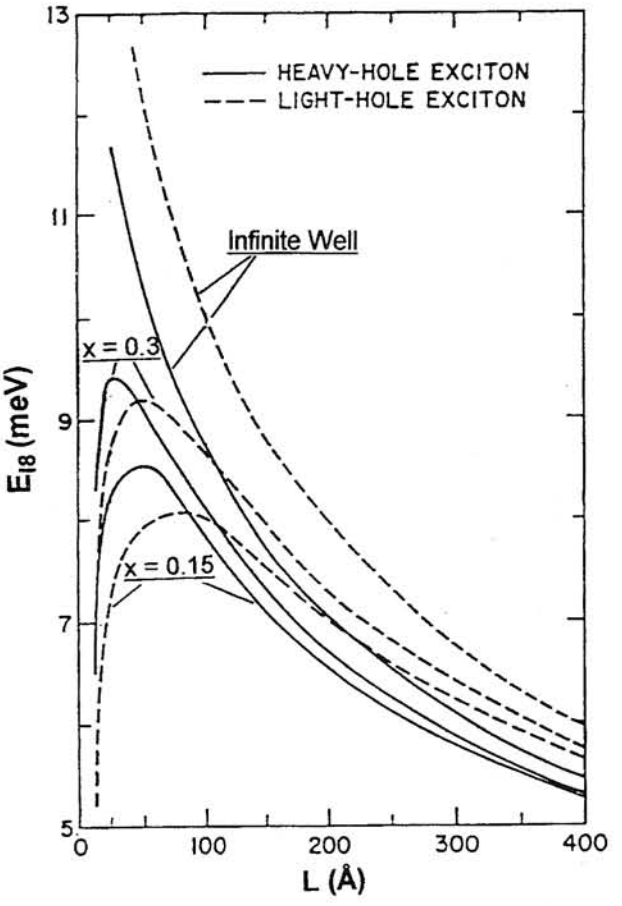

Fig.2. The calculated binding energy of $n_z = 1$ (hh) exciton in GaAs/AlGaAs quantum well as a function of well thickness L_z. According to [15].

are shifted here by the confinement energies. The subband indexes n_z have been chosen equal for electrons and holes to reflect $\Delta n_z = 1$ selection rule for the optical transitions. Some important differences in the 2D exciton properties comparing to bulk 3D excitons are illustrated by the following relations. For the binding energy E_{bin} and the radius a_1 of the lowest exciton state one finds:

$$\begin{aligned} E_{bind}^{3D} &= Ry^* \\ a_1^{3D} &= a_B \\ E_{bind}^{2D} &= 4Ry^* \\ a_1^{2D} &= a_B/2 \end{aligned} \qquad (3)$$

i.e., the excitonic effects are strongly enhanced in lowered dimensions. The properties of excitons in real quantum wells of finite depth are different from those in the ideal 2D systems [15]. The limit for $L_z \to 0$ are not ideal 2D excitons but rather 3D excitons with properties determined by barrier material. Although the exciton binding energy never reaches 4Ry* the excitonic effects are nonetheless much stronger in quantum wells than in bulk. The exciton binding energy passes through a maximum of about 2 to 3 times Ry* depending on the material parameters. The increase of the oscillator strength of 1*s* exciton comes from the fact that the quantization in *z*-direction increases both the overlap between electron and hole and their attraction, which results in turn in a reduction of two-dimensional Bohr radius. This is the reason why we observe 2D excitonic effects up to the room temperature. The Sommerfeld factor F, which describes the enhancement of the oscillator strength of the continuum states and which arises from residual electron-hole correlation, depends also on dimensionality [16].

$$F_{3D} = \frac{\pi}{W^{1/2}} \frac{e^{\pi W^{-1/2}}}{\sinh\,(\pi W^{-1/2})} \text{ with}$$

$$W = (E - E_g)\, Ry^{*-1} \qquad 4)$$

$$F_{2D} = \frac{e^{\pi W^{-1/2}}}{\cosh\ (\pi W^{-1/2})} \quad \text{with}$$
$$W = (E - E_g + E_{nz,e} + E_{nz,h})\ Ry^{*-1} \qquad (5)$$

In the three-dimensional case it has a square-root singularity at E_g and decreases gradually to unity for $\hbar\omega > E_g$. In two dimensions it decays only from two to one with increasing energy. Typical absorption spectra of GaAs/AlGaAs quantum well system are shown in Fig. 3. The absorption follows the step-like density of states in 2D system with distinct heavy hole (hh) and light hole (lh) exciton resonance just below each step. The increasing broadening of the absorption lines with subband number can be partly attributed to the fast dissociation of the excitons, which are isoenergetic with continuum states of the lower laying subbands. The luminescence spectra of excitons in quantum wells are generally less complicated. The optical transitions from lowest laying states are the only one observed, due to the termalization effects and they are usually Stokes-shifted with respect to the absorption. The exciton luminescence in the undoped quantum wells will be discussed in considerable details in the next Section.

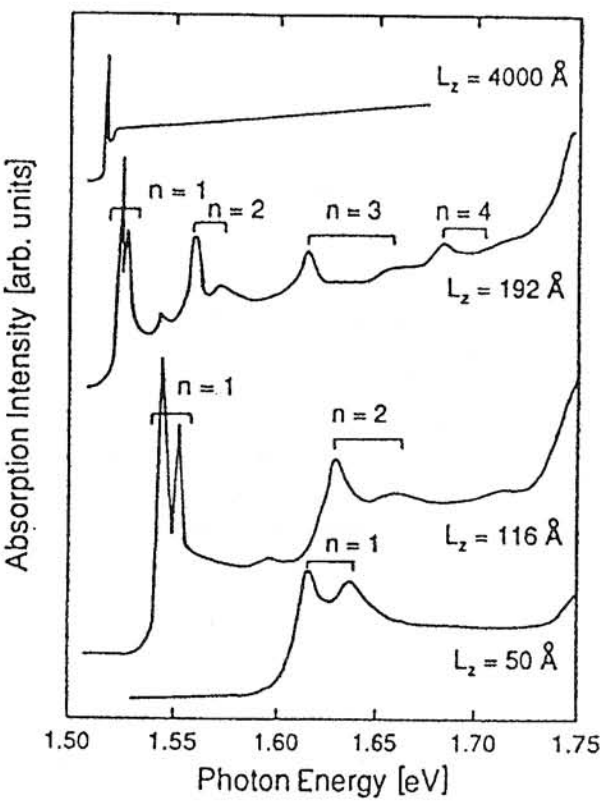

Fig. 3. Optical absorption in GaAs/$Al_{0.25}Ga_{0.75}As$ quantum wells with different thickness, demonstrating the strong excitonic resonances [17].

3. Exciton dynamics in quantum wells

Excitons in semiconductors play an important role in optical properties at low temperatures. In bulk GaAs, the binding energy of free excitons is about 4 meV and immediately after creation they tend to localize at lattice imperfections forming bound excitons. In the case of an exciton in quantum well, the two-dimensional (2D) exciton has a large binding energy and strong oscillator strength comparing to those of its three-dimensional counterpart. These are explained in terms of quantum confinement of the wave functions by the potential barriers. Moreover, the intrinsic nature of 2D excitons is greatly enhanced as opposed to 3D case. Exciton dynamics in AlGaAs/GaAs quantum wells (QW) has been widely investigated [18–29], nevertheless only very recently one has begun to get quantitative understanding of exciton recombination mechanisms and some aspects of these phenomena need further study to be fully elucidated.

3.1. Experimental details

We will report here the results of the studies performed on AlGaAs/GaAs multiple-quantum-well (MQW) structures grown by molecular beam epitaxy on Riber 32P machine at the Institute of Electron Technology in Warsaw. The samples were grown at 630°C with growth interrupts of 60 sec on each interface, on semi-insulating [100]-oriented GaAs substrates (Sumitomo), with a misorientation of $\pm 0.5°$. The samples consisted of 6 quantum wells of nominal thickness 6ML, 8ML, 12ML, 15ML, 20ML and 30ML (1ML = $a/2$ = 2.83Å) separated by 250Å thick Al_xGaAs_{1-x} (x = 0.3) barriers, and covered with 0.1 μm GaAs cap layer. The structures without growth interrupts at heterointerfaces were also grown to facilitate comparison. They consisted of 4 quantum wells of thickness 25Å, 50Å, 100Å and 200Å separated by 0.1 μm thick $Al_xGa_{1-x}As$ (x = 0.3) barriers. The MQW structures were not intentionally doped.

We have measured both continuous wave photoluminescence (PL) and photoluminescence excitation (PLE) spectra at low temperatures to examine the quality of the samples. Dynamics of exciton recombination in quantum wells of different thickness was studied at the temperature range 2K–140K by time-resolved luminescence experiments. The PL kinetics measurements were performed with a Hamamatsu synchroscan camera with a temporal resolution of about 20 ps. Pulsed excitation was provided by a dye laser synchronously pumped with a mode-locked argon laser to give pulse lengths of about 5 ps duration. The PLE measurements and time-resolved PL measurements were performed at The Department of Physics and Measurement Technology, Linköping University, Sweden.

3.2. Time resolved spectroscopy of excitons in thin quantum wells

High quality samples were used in this study, characterized by narrow PL lines and zero (or near zero) Stokes shifts between PL and PLE spectra. Low temperature photoluminescence spectrum, typical for the samples grown with growth interruptions at the interfaces, is shown in Fig.4. We can observe distinct monolayer splitting of PL lines attributed to the well with certain nominal thickness, due to the well thickness fluctuations by ± 1ML, characterized by spatial extension greater than exciton radius. The halfwidth of individual lines varies from 1.5 meV for 30ML thick well to 3.5 meV for 10ML well. Each line in the spectrum has been assigned an exact value of well thickness on the basis of theoretical calculations of energy levels in the quantum wells. The calculations have been performed within the envelope function approximation scheme developed by Bastard [30], with band nonparabolicity corrections included [31]. The positions of exciton lines have been determined as a difference between appropriate electron and hole levels minus, well thickness dependent, exciton binding energy taken from the caculations of Green *et al.* [15].

In the case of the structures grown without growth interruptions the lines are strongly inhomogenously broadened due to the well thickness fluctuations with the characteristic length scale small comparing to the exciton diameter. Their thickness

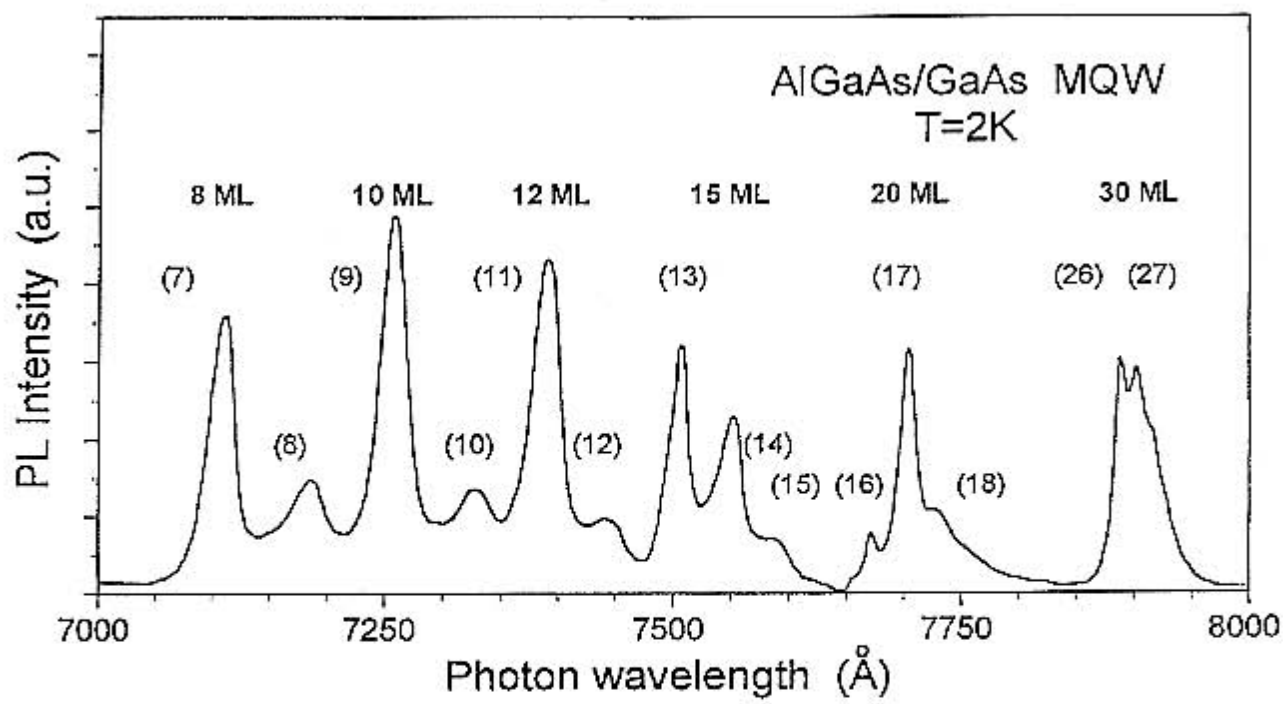

Fig. 4. Photoluminescence (PL) spectrum of multi-quantum well (MQW) structure grown with growth interruptions at the interfaces (T = 2K). Numbers in parentheses designate exact well thicknesses determined by comparing peak positions with calculated values (as described in the text). Also indicated are the values of nominal well thickness (bold numbers).

varies from 2.5 meV for 100Å thick well to 10 meV for 25Å thick well and no monolayer splitting is observed. Assuming the fluctuation of the well width to be the half of lattice constant *a* of GaAs and noting that the level energy in a quantum well scales approximately to the inverse square of the well thickness one can calculate the fluctuation of 1*s* exciton energy as:

$$\delta E_{n=1}(1s) \cong 2E_{n=1}\,(\delta L_z/L_z) \doteq 2E_{n=1}(a/2L_z) \qquad (6)$$

where $E_{n=1}(1s) = E_p\,(L_z) - E_g$ is the exciton energy measured from the bottom of the GaAs well. Taking as an example 50Å well one gets 9.8 meV for the fluctuation of exciton energy, which is of the order of observed halfwidth of PL line. For the 100Å thick well Eq.(1) gives 1.4 meV and at about 150Å the inhomogenous contribution to the broadening of exciton linewidth becomes negligible. In the case of the first type of quantum wells, grown with the interruptions at the interfaces one can attempt more detailed analysis due to mentioned earlier possibility of precise determination of actual well thickness. In Fig. 5 spectra of photoluminescence excitation (PLE) and photoluminescence (PL) for the 13ML thick well are compared. Peaks of the luminescence and photoexcitation for heavy-hole exciton $(HH)_1$ are separated by only 1.1 meV. For 17ML thick well the Stokes shift is even smaller and equals 0.5 meV. This fact indicates the high quality of the interfaces of quantum wells. With the inhomogenous contribution to the line broadening being so small we can expect that excitons recombining in such wells will manifest predominantly their intrinsic properties as opposed to quantum wells with rough interfaces or bulk material.

The energy- and time-resolved results of PL measurements for the representative examples of wells grown with and without growth interruptions at

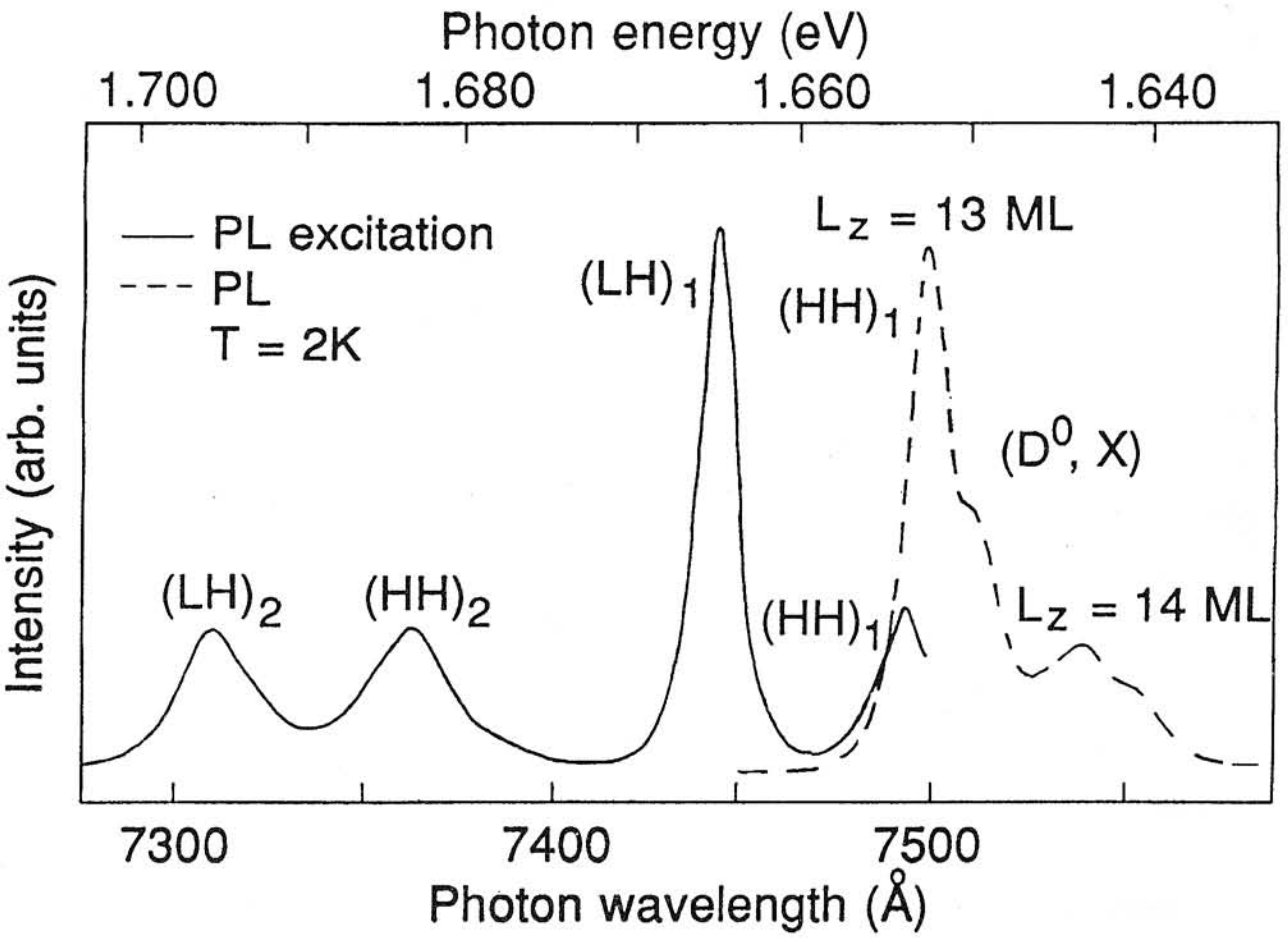

Fig. 5. Photoluminescence (PL) and Photoluminescence excitation (PLE) spectra for 13ML thick quantum well at T = 2K.

interfaces are shown in Fig. 6 and Fig. 7. These figures show contours of constant PL intensity on the energy-time plane. The energy and time response of luminescence directly reflects dynamics of exciton population. In the 50Å thick, non-interrupted quantum well peak of $(HH)_1$ exciton line moves, in about 1 ns time from its initial position at 1.606 eV, down in energy by 2.5 meV, which means that excitons drift in a well plane towards lower energy states loosing their potential energy. The build up of exciton population takes about 150 ps. The decay of the luminescence does not show single exponential behaviour; moreover it depends on energy increasing as one goes from low to high energy tail of the line. This proves that excitons below certain energy in low energy tail of the line are localized by potential fluctuations resulting from the well thickness variations, while those at higher energies move more or less freely in the well plane. A characteristic time to decay to $1/e$ value of the maximum at the peak of the line is about 180 ps for 50Å well and about 220 ps for 100Å well. On the contrary the 13 ML thick, growth interrupted well (see Fig. 7) shows negligible small (0.7 meV) shift of exciton line with time and 17 ML quantum well shows no shift at all. This means that for these wells a little trapping at the interface occurs. The decay at the peak of the luminescence line for discussed wells clearly shows two components (Fig. 8). The fast one which can be attributed to the decay of free excitons and the slow one due to the decay of localized excitons. The time constant of the fast part of the decay is equal to 140 ps for 13 ML well and 125 ps for 17 ML well, while the slow part is roughly 350–400 ps in both cases.

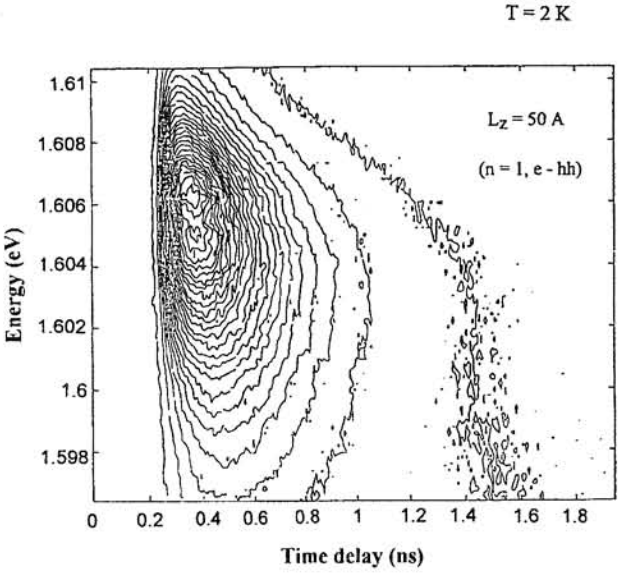

Fig. 6. The contour of constant PL intensity of excitons (n = 1, e-hh), on energy-time plane, in 50Å thick quantum well grown without growth interrupts at T=2K.

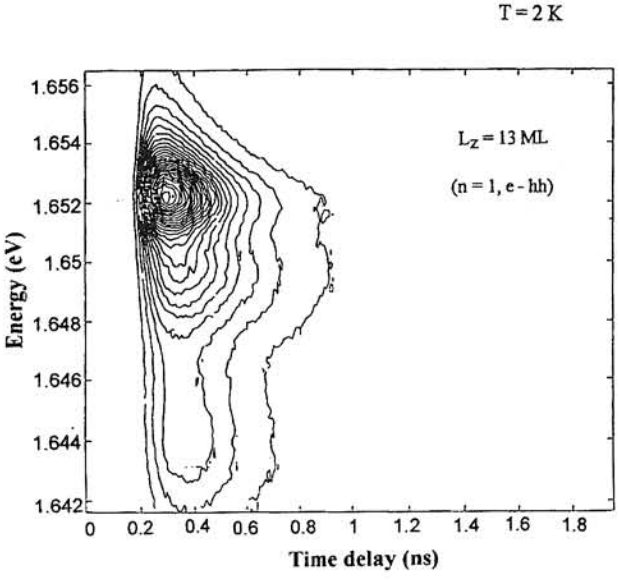

Fig. 7. The contour of constant PL intensity of excitons (n =1, e-hh), on energy-time plane, in 13ML thick quantum well grown with growth interrupts at T = 2K.

The difference of decay rate between free excitons and localized excitons results from the

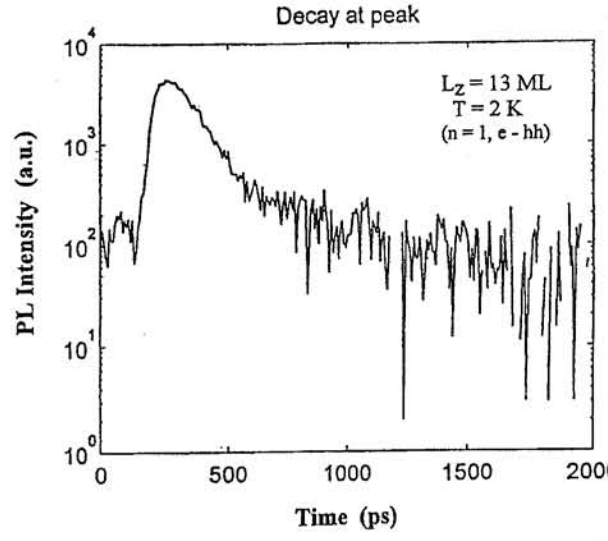

Fig. 8. The decay of the luminescence for the peak of (n = 1, e-hh) exciton line in 13ML thick quantum well at T = 2K.

difference in coherence length of both types of excitons. In the ideal quantum well at low temperatures, a free exciton is a coherent excitation of the whole crystal, leading to the large dipole transition probability and fast radiative decay rate, since the transition probability is proportional to the area of coherent excitation [32]. In the real crystal, however, free exciton has a finite coherence length due to dephasing scattering processes. The coherent area of localized exciton is even smaller, determined by spatial extend of localized state. Thus the radiative decay time of localized excitons at low temperatures should be longer than that of free excitons, both being in real crystal considerably longer than theoretical limit.

As it has been shown, in the best quality quantum wells used in this study, even at low temperatures radiative decay is dominated by free excitons. When the temperature is raised one would expect, according to simple model of Feldman *et al.* [20], that the lifetime of free excitons will increase with temperature while that of localized excitons will remain unchanged. Excitons localized by fluctuations in the well width can be formally treated as bound excitons [33]. In Fig. 9, we show the results of time- and energy-resolved measurements for 13 ML and 14 ML quantum wells taken at 60 K. The peak positions of the exciton lines remain unchanged over the whole time range and decay times for both lines are considerably longer than those at 2 K; they are equal to 490 ps and 510 ps, respectively. Moreover the decay of the luminescence is purely exponential over two decades of signal intensity as it can be seen in Fig. 10 showing PL decay for the peak of exciton line in 13 ML quantum well.

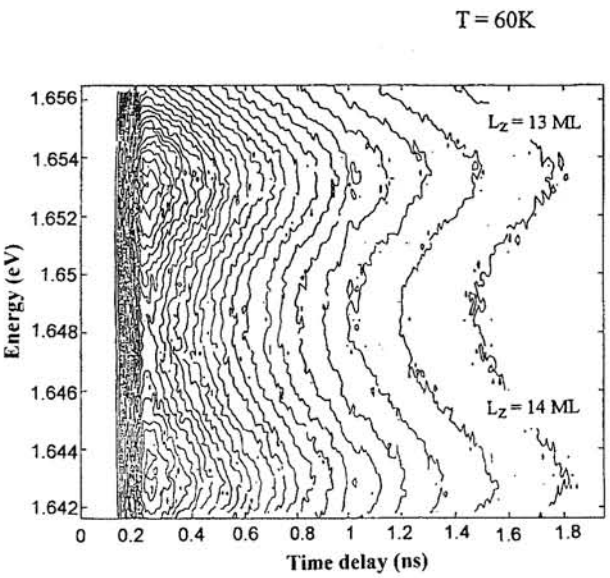

Fig. 9. The contour of constant PL intensity of excitons (n =1, e-hh), on energy-time plane, in 13ML and 14ML thick quantum wells grown with growth interruptions at T = 60K.

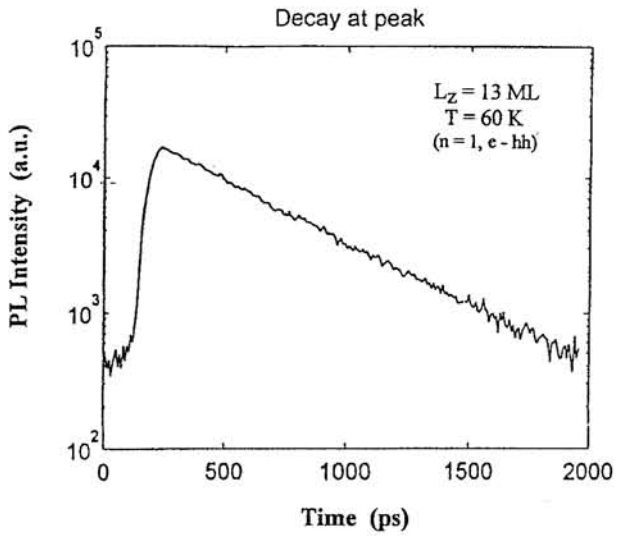

Fig. 10. The decay of the luminescence for the peak of (n =1, e-hh) exciton line in 13ML thick quantum well at T = 60K.

3.3. The lifetime of free excitons in quantum wells

The lifetime of free excitons in quantum well can be calculated under the assumption that the wavevector **k** along the plane is conserved. In bulk crystals excitons interacting with light produce mixed modes (polaritons) which are stationary. In quantum wells, because of the braking of the translational symmetry along the growth axis *z*, an exciton with wavevector **k** is coupled by the dipole interaction to photons with $\mathbf{q} = (k, k_z)$, with the same in plane wavevector but with all possible values of k_z. Only excitons with $k < k_o$ where $k_o = n\omega/c$ can recombine radiatively. Assuming further that thermalization processes are much faster than radiative recombination, Andreani *et al.* [34] have calculated the lifetime of thermalized excitons:

$$\tau_{th}(T) = \frac{3Mk_BT}{\hbar^2 k_0^2}\,\tau_0 \qquad (7)$$

where $M = m_e + m_h$ is the center of mass motion exciton mass, k_B is the Boltzman constant and τ_o is the lifetime of free excitons in the radiant state, i.e., at $k = 0$. Eq.(7) predicts an effective lifetime which varies linearly with temperature and which can be significantly longer than τ_o since only a small fraction of excitons occupy the states with $k < k_o$ which can decay radiatively (for thermal distribution of excitons only a small fraction of the states lie below the crossing with the photon dispersion line). The value of radiative lifetime τ_o calculated by Andreani equals 25 ps and is an order of magnitude longer than 2.8 ps predicted by Hanamura [32]. Using our experimental data for effective time decay of thermalized excitons we get from Eq.(2), with exciton mass $M = 0.25\ m_o$ [28], the following values of radiative lifetime τ_o: 24.4 ps for 13 ML quantum well and 21.8 ps for 17 ML quantum well. These values are very close to theoretical estimates given by Andreani [34], although they are shorter than typically reported for quantum wells (see Ref. 3). Such short lifetimes have been observed recently by Sermage *et al.* [20], who measured 18 ps in 58 Å thick GaAs well sandwiched between AlAs barriers. It seems that this theoretical predictions are reasonably accurate while the scatter of reported experimental values can be attributed to the variable quality of the interfaces in quantum wells. As long as there is no significant trapping of excitons at the interfaces and they move freely in plane of the well the above discussed model works correctly. However, allowing for week localization of excitons by well width fluctuations, as it has been done by Citrin [35], shows that due to finite scattering lifetime (dephasing) and finite spatial coherence, the radiative lifetime can be in some cases considerably longer than predicted in Ref.34. In the light of these results one can understand the apparent discrepancies between published experimental data.

3.4. Inter-island energy transfer and in-plane exciton migration in quantum wells

Structural disorder in quantum wells may result in the formation of QW regions (islands) differing in width by 1 ML, with size comparable to or larger than the exciton radius. We suggest that at low temperatures excitons in thin GaAs quantum wells prepared without growth interruptions, after loosing an excess kinetic energy are localized with potential energy determined by the local environment. Localized excitons are in a local minimum of energy and their decay is dominated by migration between localization states accompanied by absorption or emission of acoustic phonons. We observed a few meV shifts of PL lines with time, towards lower energies in this case. The temperature studies show that excitons start to move freely in the well plane at higher temperatures (~60K).

We will present here the first experimental results demonstrating existence of inter-island migration of excitons. The characteristic time scale of the process is also determined. By selectively exciting the PL (SPL spectrum) it is possible to resolve PL features related to excitonic recombination within islands differing in width by one monolayer. Fig. 11 shows the PLE spectrum measured for the detection set at the FE 24 ML emission (1.5854 eV PL) (a) and at the DBE 25 ML emission (1.5802 eV PL) (b). The assignment of the various lines is based on the theoretical calculation of the transition energies for relevant states of the HH and LH excitons in the quantum wells investigated. The sharp PLE peak at 1.5869 eV (Fig. 11a) is assigned to the HH free exciton peak of the FE 24 ML emission, with the accompanying LH exciton peak observed at higher energy. The PLE spectrum detected at the DBE 25 ML PL (Fig. 11b) contains an additional HH exciton peak at 1.5831 eV, identified as the HH FE 25 ML. We explain the appearance of this peaks by the exciton migration from 24 ML to 25 ML thick islands in the quantum well plane. To quantify our description of the inter-island exciton migration we have decomposed the time-resolved PL spectra into three (for resonant excitation) and two (for non-resonant excitation) Gaussian components and traced they time and intensity evolution. The relevant results are shown in Fig. 12. The PL decay times of the individual PL subbands were determined as 115 ps for the FE 24 ML emission and 190 ps for the FE 25 ML emission. The 75 ps difference between the decay times of the two FE emissions is to large to be explained by the difference in the radiative decay time of two QWs differing in the width by only one monolayer [1]. We relate it to inter-island exciton migration, which reduces the decay time of FE 24 ML

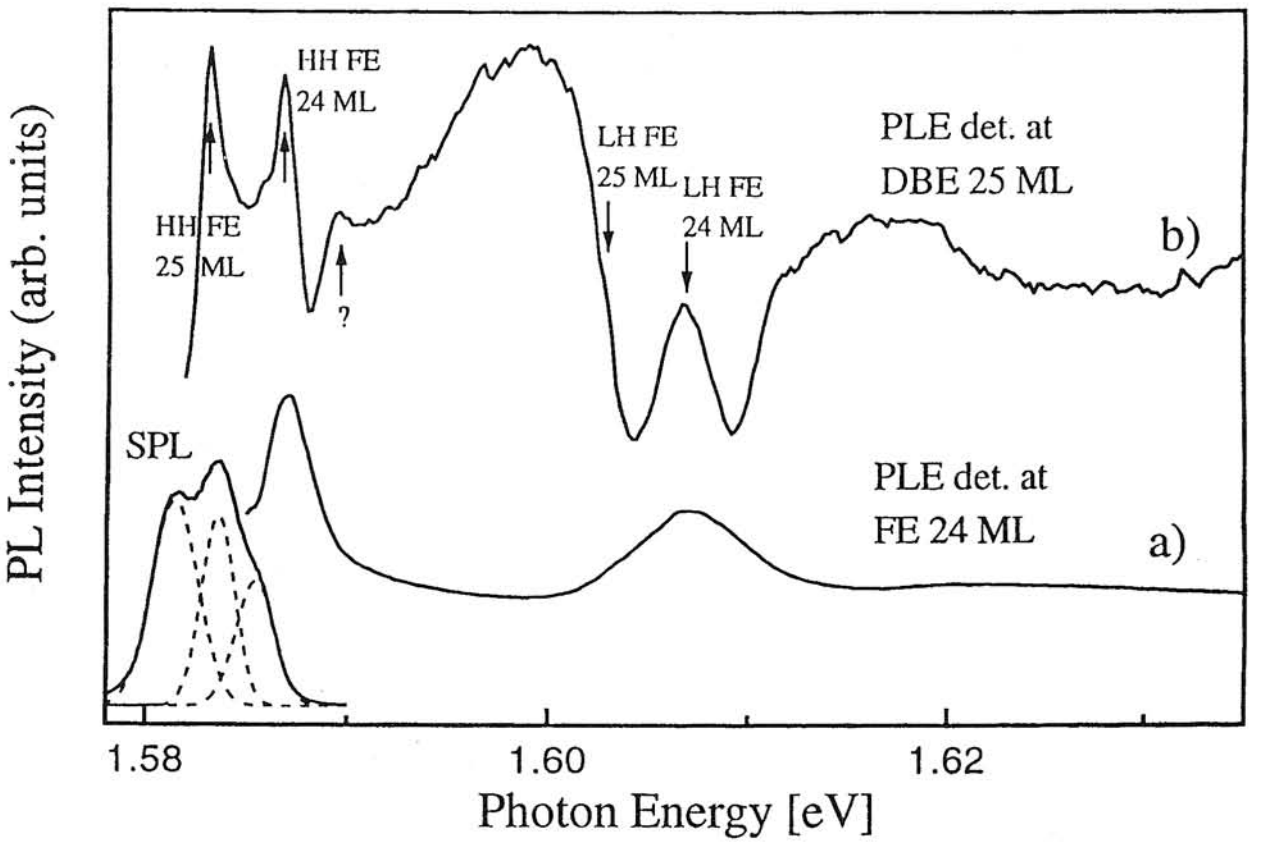

Fig. 11. PLE spectrum for detection energy set at: (a) the peak of the free-exciton (FE) 24 ML emission (1.5836 eV) and (b) the peak of the donor-bound exciton (DBE), 25 ML emission (1.5802 eV).

photoluminescence. From the linear rate equations we have derived the exciton transfer rate from the 24 ML to the 25 ML region to be approximately 290 ps^{-1}. In addition to the inter-island exciton migration, we have also observed a relatively slow exciton drift-diffusion between QW states of a slightly different potential energy. This was observed as a shift of PL lines spectral positions, towards lower energies, during the exciton decay time.

In the growth-interrupted quantum wells in which the size of islands with constant well thickness is large compared with exciton diameter we observe splitting of the heavy-hole transitions into the multiplets of narrow lines corresponding to one monolayer differences in the well width. The energy shifts with time are observed in this case only for the narrowest wells (L_z) and amount to only a fraction of the width of individual lines suggesting the inter-island migration of excitons mediated by acoustic phonon scattering as being responsible for the final stage of exciton relaxation. Two-step decay of the luminescence is observed at low temperatures (2K) for these wells. The fast part of the decay was attributed to the decay of free excitons whereas the slow one is believed to be due to the decay of the excitons localized at the interfaces. However, in most cases in best quality growth-interrupted quantum wells we observed predominantly free exciton recombination. Temperature dependent measurements show that at higher temperatures luminescence decay becomes governed by single exponential as expected, for delocalized excitons (no energy shift is observed).

The interface roughness and compositional fluctuations are well known to provide changes in the QW potential profile that can scatter or even localize excitons. As long as localization is concerned we can practically eliminate it in best QWs. Even in atomically flat interfaces, there remains, however, certain amount of microroughness which can scatter excitons, as evidenced by TEM [36] and resonant-Raman scattering [37] studies.

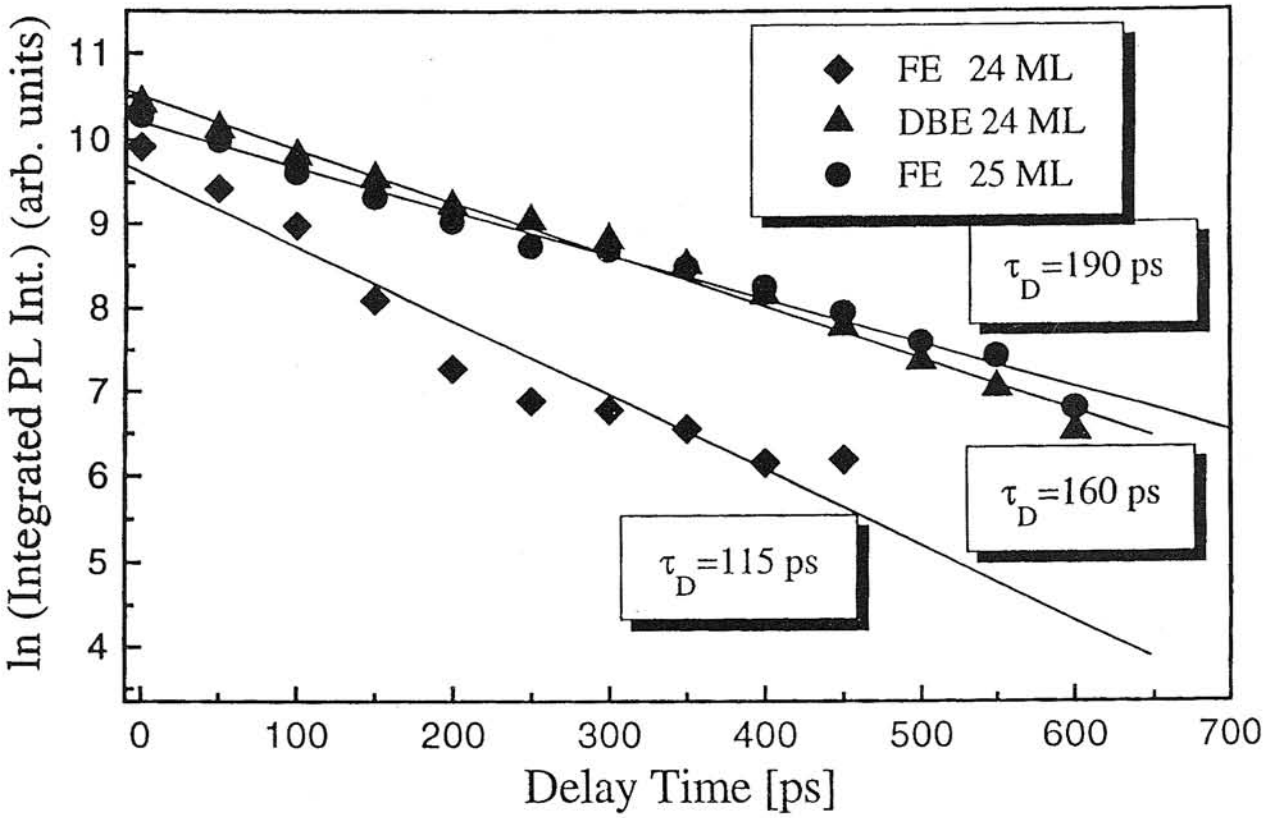

Fig. 12. PL kinetics of the three emission lines: FE 24 ML, DB 24 ML and FE 25 ML obtained from the dependence of integrated PL intensity on delay time in the time-resolved PL experiment under resonant excitation.

The influence of this scattering on optical properties of QWs, to be fully understood, needs further experimental and theoretical investigations.

4. Many-body effects in quantum wells

4.1. Beyond the independent-electron approximation [38]

The problem of electrons in a solid is in principle a many electron problem, for the full Hamiltonian of the solid contains not only the one-electron potentials describing the interactions of the electrons with the atomic nuclei, but also pair potentials describing the electron-electron interactions. In the independent electron approximation these interactions are represented by an effective one-electron potential $U(\mathbf{r})$ in Schrödinger equation. Writing down a separate Schrödinger equation

$$\left(-\frac{\hbar^2}{2m}\nabla^2 + U(r)\right)\psi_k(r) = E(k)\,\psi_k(r) \quad (8)$$

for each electron is, however, an enormous simplification of the actual problem of many interacting electrons in a periodic potential. In an exact treatment each electron cannot be described by a wave function determined by the single-particle Schrödinger equation, independent of all the others. A more accurate calculation of the electronic properties of solid should start with the Schrödinger equation for the N – particle wavefunction for all N electrons in the solid $\Psi(\mathbf{r}_1,\mathbf{s}_1,\mathbf{r}_2\mathbf{s}_2,\ldots,\mathbf{r}_N\mathbf{s}_N)$:

$$H\Psi = \sum_{i=1}^{N}\left(-\frac{\hbar^2}{2m}\nabla_i^2\Psi - Ze^2\sum_{R}\frac{1}{|r_i - R|}\Psi\right) + \frac{1}{2}\sum_{i\neq j}^{N}\frac{e^2}{|r_i - r_j|}\Psi = E\Psi \quad (9)$$

Here the negative potential-energy term represents the attractive electrostatic potentials of the

bare nuclei fixed at the points **R**, and the last term represents the interactions of the electrons with each other. Evidently $U(\mathbf{r})$ should include the potential of the ions:

$$U^{ion}(\mathbf{r}) = -Ze^2 \sum_{R} \frac{1}{|r_i - R|} \qquad (10)$$

In addition $U(\mathbf{r})$ should incorporate (at least approximately) fact that the electron feels the electric fields of all other electrons. Treating the remaining electrons as a smooth distribution of negative charge with charge density ρ, the potential energy of the given electron in their field would be:

$$U^{el}(\mathbf{r}) = -e\int d\mathbf{r}'\rho(\mathbf{r}') \frac{1}{|\mathbf{r} - \mathbf{r}'|} \qquad (11)$$

The contribution of an electron in the state ψ_i to the charge density is: $\rho_i(\mathbf{r}) = -e\,|\psi_i(\mathbf{r})|^2$ and the total charge density would than be: $\rho(\mathbf{r}) = -e\sum_i |\psi_i(\mathbf{r})|^2$, where the sum extends over all occupied one-electron levels in the solid. Taking the above into account we arrive at the one-electron equation:

$$-\frac{\hbar^2}{2m}\nabla^2\psi_i(\mathbf{r}) + U^{ion}(\mathbf{r})\psi_i(\mathbf{r}) + \left[e^2\sum_j \int d\mathbf{r}'\,|\psi_i(\mathbf{r}')|^2 \frac{1}{|\mathbf{r} - \mathbf{r}'|}\right]\psi_i(\mathbf{r}) = \varepsilon_i\psi_i(\mathbf{r}) \qquad (12)$$

Actually this is a set of equations, one for each occupied one-electron level $\psi_i(\mathbf{r})$, known as the Hartree equations. These nonlinear equations for the one-electron wave functions and energies are solved iteratively. The simplest solution to the Eq.12 would be a product wave function of the form:

$$\Psi(\mathbf{r}_1s_1, \mathbf{r}_2s_2, ..., \mathbf{r}_Ns_N) = \psi_1(\mathbf{r}_1s_1)\psi_2(\mathbf{r}_2s_2)...\psi_N(\mathbf{r}_Ns_N) \qquad (13)$$

where the ψ_i are a set of N orthonormal one-electron orbitals. There are, however, certain important physical features of electron-electron interactions that can not be treated in a simple self-consistent field (Hartree) approximation. These are phenomena known as "exchange" and "screening". The wave function (13) is incompatible with Pauli exclusion principle, which requires the sign of Ψ to change when any two of its arguments are interchanged. The simplest generalization of the Hartree approximation that incorporates the antisymmetry requirement is to replace trial wave function of Eq.13 by a Slater determinant of one-electron wave functions.

$$\Psi(\mathbf{r}_1s_1, \mathbf{r}_2s_2, ..., \mathbf{r}_Ns_N) = \begin{vmatrix} \psi_1(\mathbf{r}_1s_1)\psi_1(\mathbf{r}_2s_2)...\psi_1(\mathbf{r}_Ns_N) \\ \psi_2(\mathbf{r}_1s_1)\psi_2(\mathbf{r}_2s_2)...\psi_2(\mathbf{r}_Ns_N) \\ ..... \\ ..... \\ \psi_N(\mathbf{r}_1s_1)\psi_N(\mathbf{r}_2s_2)...\psi_N(\mathbf{r}_Ns_N) \end{vmatrix} \qquad (14)$$

The wave function of the form given by Eq.14 leads to a generalization of Hartree equations known as the Hartree-Fock equations:

$$-\frac{\hbar^2}{2m}\nabla^2\psi_i(\mathbf{r}) + U^{ion}(\mathbf{r})\psi_i(\mathbf{r}) + U^{el}(\mathbf{r})\psi_i(\mathbf{r}) - \sum_j \int d\mathbf{r}' \frac{e^2}{|\mathbf{r} - \mathbf{r}'|}\psi_i(\mathbf{r})\,\psi_j^*(\mathbf{r}')\psi_i(\mathbf{r})\delta_{s_is_j} = \varepsilon_i\psi_i(\mathbf{r}) \qquad (15)$$

where U^{el} is defined by Eq.11. This equations differ from the Hartree equations (12) by an additional term on the left hand side known as the exchange term which leads to correlated behaviour of electrons having parallel spin alignment. The complexity introduced by the exchange term is considerable. Unlike the self-consistent field (direct) U^{el} term, the exchange term is not of the $V(\mathbf{r})\psi(\mathbf{r})$ form; instead it is an integral operator of the type $\int V(r, r')\psi(r')dr'$. As a result Hartee-Fock equations are in general intractable except for the case when periodic potential is zero or constant (free electron gas). The electrons with equal spins repel each other as a consequence of Pauli exclusion principle. Thus, each electron is surrounded by an exchange hole, i.e., by a net positive charge distribution. The exsistence of exchange hole expresses the fact that mean separation between electrons with equal spins is larger that it would be without the Pauli exclusion principle. For the interacting electron gas, the increased separation between repulsive charges reduces the overall Coulomb interaction. This is because of the attractive interaction of electron with its own exchange

hole. That interaction reduces the total energy of the system by the amount [39]:

$$E_{pot}^{HF} = E_{exc} = -\frac{e^2L^3}{4\pi^3\varepsilon_0}(3\pi^2n)^{4/3} \qquad (16)$$

The total Hartree-Fock energy is equal to the sum of kinetic energy E_{kin}^{HF} and the above interaction energy: $E_0^{HF} = E_{kin}^{HF} + E_{pot}^{HF}$. The kinetic energy can be evaluated as:

$$E_{kin}^{HF} = \frac{\hbar^2L^3}{10m\pi^2}(3\pi^2n)^{5/3} \qquad (17)$$

According to Hartree-Fock theory, electrons with different spin do not avoid each other, since the states are chosen to satisfy the exchange principle but they do not include Coulomb correlations which lead to the so-called Coulomb hole. To treat these correlation effects, one has to go beyond Hartree-Fock theory, e.g., using screened Hartree-Fock approximation [40]. Generally one can write the exact ground state energy E_0 as

$$E_0 = E_0^{HF} + E_{cor} = E_{kin}^{HF} + E_{exc} + E_{cor} \qquad (18)$$

An exact calculation of E_{cor} is generally not possible. To get good estimates of correlation energy is one of the tasks of many-body theory [41].

The major manifestation of many-body interaction in dense electron/hole plasmas is band-gap renormalization. The frequent approach to the treatment of these phenomenon is the *random-phase approximation* (RPA). The corrections to the single particle energies which have been so far splitted into two terms, i.e., *Coulomb-hole* and *screened-exchange* in the language of field theory are represented by the real part of their self-energy $\sum_{e,h}(k, E_{e,h}(\mathbf{k}))$ [12]. The band-gap renormalization is given by the sum of self-energies for electrons and holes at band edges ($k = 0$, $E = 0$)

$$\Delta = \mathrm{Re}\sum_e(0,0) - \mathrm{Re}\sum_h(0,0) \qquad (19)$$

The single-particle self-energy is given in RPA by the convolution of the single particle Green's function and dynamically screened Coulomb interaction treated in a single-plasmon-pole approximation.

4.2. Fermi-edge singularity in excitonic spectra of quantum wells containing high density electron plasma

The one-component plasmas, i.e., plasmas consisting predominantly of electrons or holes provide an easy way to study many body interactions in semiconductors. Such situations are achieved by heavy doping of semiconductor materials beyond the metallic limit. Optical studies of the many body phenomena involve the generation of additional electron-hole pairs; usually in concentrations much smaller than that of electron or hole plasma. For, let us say, n-type material the number of electrons remains practically unchanged in such situation, whereas the number of holes is determined by optical excitation. The holes then display some correlation effects, while the exchange effects are negligible unless very high excitation intensities are reached. Additional large contributions to the screening and renormalization effects arise from the interaction of the free carriers and the ionized impurities. A clear cut situation arises when the free carriers are spatially separated from the parent impurities. Such a separation can be realized in 2D modulation doped structures where the dopant atoms are localized in the barriers and the free carriers are spatially confined in a quantum well [12].

4.2.1. Modulation doped quantum wells

Modulation doped heterostructures [42] provide an excellent means for the realization of a 2D electron or hole gas and have shown many remarkable new physical phenomena. They are also attractive from the device point of view. Much of their significance results from the fact that-unlike in doped bulk semiconductors- the carriers are spatially separated from their parent impurities, which results in extremely high carrier mobilities (generally in excess of $10^6 cm^2V^{-1}s^{-1}$). Fig. 13 shows the band structure of a typical (n-type) modulation-doped quantum well structure (MDQW). During the growth, the dopants are restricted to the barrier material. In order to maintain a constant Fermi energy throughout the sample, they ionize with the free carriers migrating to the lower-energy quantum well. The charge transfer creates significant electric fields. In the framework of density functional theory [43] potential V_{XS} felt by a carrier consists of several parts

$$V_{XS}(z) = V(z) + V_H(z) + V_{XC}(z) \qquad (20)$$

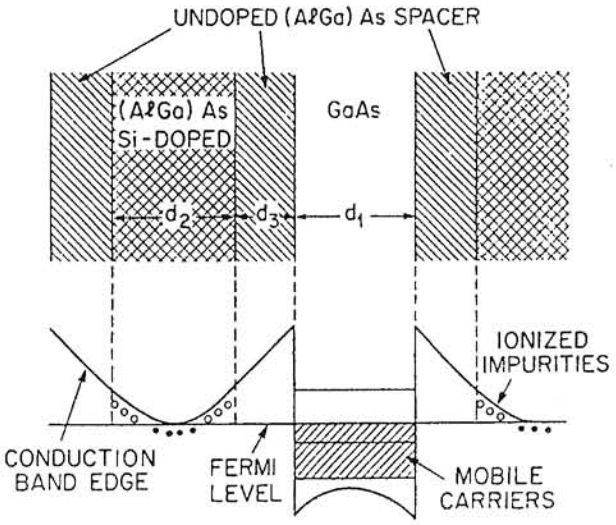

Fig. 13. Relative position of the conduction band edges in n-type modulation doped GaAs/AlGaAs quantum well structure.

The first term, V, is the bare square-well potential determined by the band offset. The Hartree potential, V_H, consists of the electrostatic potential due to the ionized impurities and free carriers. Throughout Poisson's equation it depends in turn on the local carrier density and thus has to be determined self-consistently. It gives rise to the band bending shown in Fig. 13. For n-type MDQW one has:

$$\frac{d^2}{dz^2}V_H(z) = -\frac{4\pi e^2}{\varepsilon_0}[\rho_e(z) - N^+_D(z)] \quad (21)$$

where $\rho_e(z)$ and $N^+_D(z)$ are electron and the ionized donor densities, respectively. The Eq.(21) has to be solved self-consistently with Schrödinger equation [44]. If $\rho_e(z)$ is approximated by the homogeneous density N/L_z inside the QW we get:

$$V_H(z) \approx -\frac{2\pi N e^2}{\varepsilon_0 L_z} z^2 \quad (22)$$

that is, the band bending varies roughly like a parabola. Finally, V_{XC} is the exchange-correlation potential which describes many-body interactions [10]. The main effect of the V_{XC} is band-gap renormalization described in Section 4.1. We shall discusse their effect on luminescence spectra of modulation doped QWs qualitatively in the subsequent Section. The main features to be explained are:

(1) The large Stokes shift between luminescence and absorption (or PL and PLE)
(2) The shape of PL spectrum (enhancement of the optical transitions at the Fermi energy)
(3) The carrier concentration and the temperature dependence of the luminescence.

We shall answer these and other questions by following Ruckenstein and Schmitt-Rink [45].

4.2.2. Many-body edge singularity in quantum-well optical spectra

The many-body properties of 2D one-component plasmas are reflected in their optical spectra. In particular the singularity of the optical spectra at the Fermi edge has been observed [46,47]. The Fermi-edge singularity (FES) or Mahan exciton [48] arises in n-type modulation doped quantum wells from the correlation between a photo-excited hole and the sea of electrons in the quantum well. Since the only electrons that can contribute to the screening of the positive hole charge are those close to the Fermi surface (no scattering can occur to the filled states with $k < k_F$) the strong enhancemet of the oscillator strength of excitonic transitions close to the Fermi level is expected.

The investigated samples were high quality modulation doped $Al_{0.3}Ga_{0.7}As/GaAs/ Al_{0.3}Ga_{0.7}As$ quantum wells grown by molecular beam epitaxy (MBE) on GaAs substrates. The schematic structure of the samples investigated is shown in Fig. 14. The samples consisted of the 100Å wells sandwiched between 1300Å thick, doped barriers barriers. The sections of the length of 200Å separated by 100Å from the edge of the well were doped with Si to the concentration $10^{18}cm^{-3}$ (sample #162.96) and $10^{17}cm^{-3}$ (sample #163.96). The samples co-doped with Be acceptors in the well were also investigated.

SAMPLES OF MODULATION DOPED $Al_{0.3}Ga_{0.7}As/GaAs$ QUANTUM WELLS GROWN BY MBE

SAMPLE NUMBER	DOPANT (Be) CONCENTRATION [cm^{-3}]	DOPANT (Si) CONCENTRATION [cm^{-3}]
#162.96	0	$1\cdot10^{18}$
#163.96	0	$1\cdot10^{17}$
#164.96	$3\cdot10^{16}$	$1\cdot10^{17}$
#165.96	$3\cdot10^{16}$	$1\cdot10^{18}$

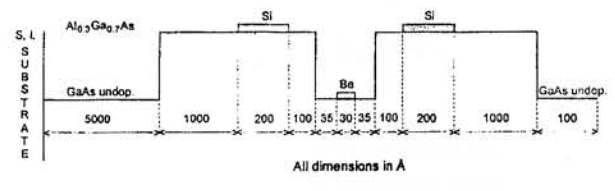

Fig. 14. The schematic structure of the modulation doped samples used in this study.

Photoluminescence (PL) and photoluminescence excitation (PLE) measurements were performed in the temperature range 2K-300K using an argon laser or Ti-saphire laser as the excitation source.

The optical absorption transitions in n-type modulation doped quantum wells (MDQW) are momentum conserving and due to the filling of the conduction band start at the energies higher than the band gap. On the other hand the emission starts at the energy equal to the effective band gap (ε_g) and extends to higher energies as far as the spread of hole k-vector allows. Thus, there is always energy shift between PL and PLE spectra, which can be clearly seen in Fig. 15. The magnitude of the Stokes shift is many times larger than

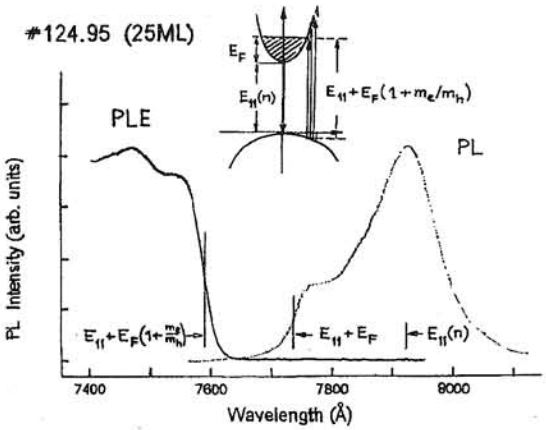

Fig. 15. PL and PLE spectra of the 25 ML thick MDQW sample donor doped in the barriers ([Si] = $10^{18}cm^{-3}$) and acceptor co-doped in the well ([Be] = $3 \times 10^{16}cm^{-3}$). The PL peak is downshifted in energy due to the concentration dependent band gap renormalization (BGR); besides that an enhancement of the PL transitions is observed at Fermi energy (E_F) The onset of PLE spectrum is shifted to higher energies by E_F and band structure related factor.

in the case of undoped quantum wells of comparable thickness; c.f. Fig. 5. In the parabolic approximation Fermi energy E_F is related to the low energy onsets of absorption (ε_F) and emission (ε_g) by:

$$E_F = (\varepsilon_F - \varepsilon_g)\ (1 + m_e/m_h)^{-1} \qquad (23)$$

where m_e/m_h is the effective mass ratio for the bands considered. Knowing the density of 2D electron gas in MDQW from the SdH oscillations one can calculate Fermi wavevector

$$k_F = (2\pi n_s)^{1/2} \qquad 24)$$

and resulting Fermi energy

$$E_F = (\hbar\pi/m_e)n_s. \qquad (25)$$

We have found an excellent agreement between the calculated and experimental values of E_F determined from PL and PLE spectra.

The low temperature PL spectrum for the sample #162.96 is shown in Fig. 16. The spectrum spreads over wide energy range and in contrast to undoped reference sample shows two well defined peaks separated by 81.6 meV. As the temperature increases the Fermi level is broadened and the high energy peak gradually disappears although it is still visible at 77K (see Fig. 17).

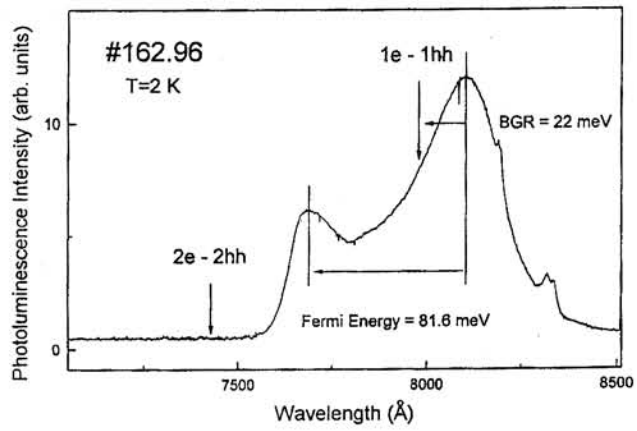

Fig. 16. PL spectrum from modulation doped quantum well of the thickness L = 100Å. The spectrum shows the strong enhancement towards the Fermi energy E_F.

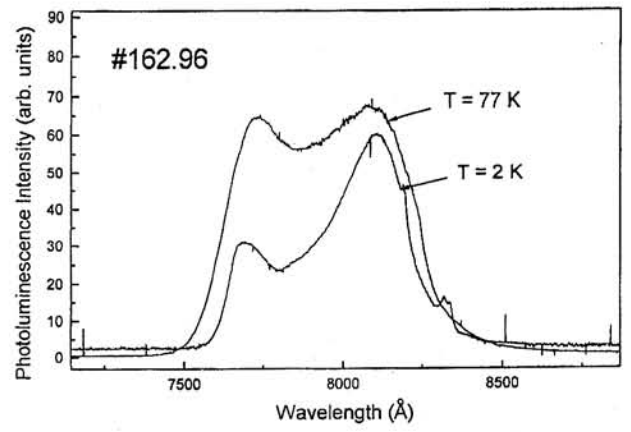

Fig. 17. Temperature dependence of PL spectrum for the 100Å thick $Al_{0.3}Ga_{0.7}As$/ GaAs/$Al_{0.3}Ga_{0.7}As$ MDQW.

A very improbable, nonthermalized electron distribution would have been needed to account for observed shape of PL spectrum if only vertical k-conserving transitions between electron and holes occurred. On the other hand an abrupt cut-off at the Fermi energy shows that the carrier temperature must be low.

To account for apparently indirect transitions violating k-selection rule we invoke the following possible mechanism. At sufficiently small separation between E_F and the next electron subband (n = 2) an efficient scattering path near k = 0 is available for electrons at the Fermi energy (see Fig. 18). This can be observed in photoluminescence as an enhancement of many-body excitonic transitions at the high energy side of the emission

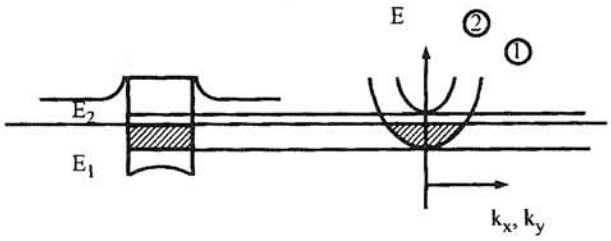

Fig. 18. Sketch of the three band model invoked in the resonant scattering description of Fermi enhancement in MDQWs.

line. Thus the access to an efficient scattering path for the electrons at the Fermi energy allows for observation of Fermi edge singularity (FES) in excitonic spectra despite the lack of localization mechanism of the holes (lack of acceptors or interface scattering providing momentum conservation). Although the separation of two peaks seen in PL spectrum shown in Fig. 16 is simple function of 2D electron density n_s the absolute position of the spectrum is not. It is indeed shifted down with respect to the undoped reference sample due to the band gap renormalization resulting from exchange interaction between electrons. The amount of band gap reduction has been estimated for 22 meV and is in agreement with local-density approximation (LDA) calculations [49]. In the narrower quantum wells for which the separation between n = 1 and n = 2 electronic subbands is higher, the above described three-band-mechanism [50], relaying on the resonant transitions from the Fermi edge into the n = 2 exciton states, is no longer operating and to observe Fermi edge enhancement of excitonic spectra we had to co-dope the samples with Be acceptors in the well, which was the case of the sample presented in Fig. 15. The localization of holes at the acceptors provided necessary spread of their wavevectors and k-conserving transitions were possible for $k \neq 0$ although in this case Fermi edge singularity was much less pronounced.

Summarizing, we have observed the FES from n-type $Al_{0.3}Ga_{0.7}As$/ GaAs/ $Al_{0.3}Ga_{0.7}As$ MDQW. The dominant mechanism responsible for the FES in Be co-doped quantum wells has been shown to be the localization of holes at the acceptors. In the case of undoped quantum wells it is the resonant scattering of electrons near the Fermi edge and the next (n = 2) unoccupied subband which produces a sufficient k = 0 admixture in exciton wavefunction and enhances transitions from the high energy states despite the lack of localization mechanism of the holes. The results are of interest from the fundamental point of view. Such effects are also important for the modelling of optoelectronic device operation under high injection conditions.

5. Conclusions

Despite the length of the article and numerous references contained therein it represents only the very introduction to the field of the optical properties of QWs, in particular the ones observed at high carrier densities which description requires the full many-body treatment. Going beyond an independent electron approximation itself requires very advanced theoretical treatment. In the article written from the experimental physicist perspective, to avoid complicated field theory formalism, we have been only able to touch upon many important issues. Our aim was to give the physical feeling rather than rigorous description of described phenomena. We almost exclusively used our own results to illustrate the presented material. It has to be also stressed that all advanced quantum structures analyzed in this article were grown in the Laboratory of Quantum Electronic Structures of The Institute of Electron Technology by molecular beam epitaxy (MBE) technique.

The research in our laboratory are device oriented; one of the main goals is the development of advanced semiconductor lasers of different construction and from variety of materials. The lasers by their nature operate at high injection conditions for which one-electron description fails. Many-body effects are most important for gain-medium properties that involve carrier density dependent changes in gain or index of refraction. Many-body effects are enhanced in 2D comparing to bulk material, making them even more important in QW lasers.

Acknowledgements

We would like to take this opportunity to acknowledge the collaboration and advice of many colleagues in our own work in the area of quantum wells. They are: Drs. P.O. Holtz, J.P. Bergman, T. Lundström, C. Ferreira from Linköping University, Prof. M. Godlewski from Polish Academy of Sciences and Dr. M. Kaniewska, M. Wesołowski, J. Muszalski from Institute of Electron Technology. We also thank Prof. B. Monemar for his generous support of collaborative research project between Linköping University and the Institute of Electron Technology.

References

1. M. Bugajski, M. Godlewski, J.P. Bergman, B. Monemar, K. Regiński, M. Kaniewska: *Exciton dynamics in thin AlGaAs/GaAs quantum wells grown by MBE*, Thin Solid Films, **267** (1995) 84.
2. M. Bugajski, K. Regiński, M. Godlewski, J.P. Bergman, B. Monemar, J. Muszalski, M. Kaniewska: *Time- and energy-resolved photoluminescence study of interface quality in AlGaAs/GaAs quantum wells*, in Semiconductor Heteroepitaxy, eds. B.Gil, R.L.Aulombard, World Scientific, Singapore, 1995.
3. M. Godlewski, P.O. Holtz, J.P. Bergman, B. Monemar, K. Regiński, M. Bugajski: *Inter-island energy transfer in AlGaAs/GaAs quantum wells grown by MBE*, Acta Phys. Polonica, **A 90** (1996) 1007.
4. M. Godlewski, J.P. Bergman, P.O. Holtz, B. Monemar, M. Bugajski, K. Regiński, M. Kaniewska: *The inter-island energy transfer in AlGaAs/GaAs quantum wells grown by molecular beam epitaxy*, Acta Phys. Polonica **A 88**, (1995) 719.
5. M. Bugajski, K. Regiński, M. Godlewski, M. Wesołowski, P.O. Holtz, A.V. Buyanov, B. Monemar: *Fermi-edge singularity in excitonic spectra of modulation doped quantum wells*, Acta Phys. Polonica **A 90** (1996) 751.
6. M. Wesołowski, M. Bugajski, K. Regiński, M. Godlewski, P.O. Holtz: *Photoluminescence and photoexcitation studies of modulation doped quantum wells*, 5th Polish-Lithuanian Workshop on the Semiconductor Physics and Technology, Vilnius 20–21.06, 1996.
7. M. Godlewski, P.O. Holtz, J.P. Bergman, B. Monemar, K. Regiński, M. Bugajski, E.M. Goldys, T.L. Tansley: *Inter-island energy transfer and i-n plane exciton migration in AlGaAs/GaAs quantum wells detected by exciton dynamics*, Superlattices and Microstructures, **20** (1996) 1.
8. M. Bugajski: *Many-body interactions in 2D electron gas; optical properties and gain*, Electron Technology, **30** (1997) no.2/3.
9. K. Regiński, M. Bugajski, J. Muszalski, M. Kaniewska, D. Radomska: *Molecular beam epitaxy of modulation doped AlGaAs/GaAs quantum well structures*, Thin Solid Films, 1997, to be published.
10. S. Schmitt-Rink, D.S. Chemla, D.A.B. Miller: *Linear and nonlinear properties of semiconductor quantum wells*, Advances in Physics, **38** (1989) 89.
11. R. Cingolani, K, Ploog: *Frequency and density dependent radiative recombination processes in III-V semiconductor quantum wells and superlattices*, Advances in Physics, **40** (1991) 535.
12. H. Kalt: *Optical properties of III-V semiconductors*, Springer Series in Solid-State Sciences **120**, Springer-Verlag, Berlin (1996).
13. *Third International Conference on Optics of Excitons in Confined Systems*, eds. G. Basterd, B. Gil, Journal de Physique IV, Colloque C5, (1993).

14. M. Shinada, S. Sugano, J. Phys. Soc. Jpn. 21, (1966) 1936.
15. R.L. Green, K.K. Bajaj, D. Phelps, Phys. Rev. **B29** (1984) 1807.
16. C.F. Klingshirn: *Semiconductor Optics*, Springer Verlag, Berlin (1995).
17. R. Dingle: *Confined carrier quantum states in ultrathin semiconductor heterostructures*, Festkörperprobleme XV, **21** (1975).
18. Y. Masumoto, S. Shionoya, H. Kawaguchi, Phys. Rev. **B29** (1984) 2324.
19. J. Kusano, Y. Segawa, Y. Aoyagi, S. Namba, H. Okamoto, Phys. Rev. **B40** (1989) 1685.
20. J. Feldman, G. Peter, E.O. Gobel, P. Dawson, K. Moore, C. Foxon, R.J. Elliott, Phys. Rev. Lett., **56** (1987) 2337.
21. M. Kohl, D. Heitmann, S. Tarucha, K. Leo, K. Ploog, Phys. Rev. **B39** (1989) 7736.
22. T.C. Damen, J. Shah, D.Y. Oberli, D.S. Chemla, J.E. Cunningham, J.M. Kuo, Phys. Rev. **B42** (1990) 7434.
23. R. Eccleston, R. Strobel, W.W. Ruhle, J. Kuhl, B.F. Feuerbacher, K. Ploog, Phys. Rev. **B44** (1991) 1395.
24. M. Zachau, J.A. Kash, W.T. Masselink, Phys. Rev. **B44** (1991) 8403.
25. M.A. Herman, D. Bimberg, J. Christen, J. Appl. Phys., **70** (1991) R1.
26. M. Colocci, M. Gurioli, J. Martinez-Pastor, Journal de Physique IV, Colloque C5, **3** (1993) 3.
27. J. Martinez-Pastor, A. Vinattieri, L. Carraresi, M. Colocci, Ph. Roussignol, G. Weimann, Phys. Rev. **B47** (1993) 10 456.
28. B. Sermage, S. Long, B. Deveaud, D.S. Katzer, Journal de Physique IV, Colloque C5, **3** (1993) 19.
29. Y. Takahashi, S.S. Kano, K. Muraki, S. Fukatsu, Y. Shiraki, R. Ito, Appl. Phys. Lett., **64** (1994) 1845.
30. G. Bastard, J.A. Brum, IEEE J. Quantum Electron., **QE-22** (1986) 1625.
31. W. Lewandowski, M. Bugajski, S.D. Hersee, Electron Technology **21** (1988) 83.
32. E. Hanamura, Phys. Rev. **B38** (1988) 1228.
33. T. Takagahara, E. Hanamura, Phys. Rev. Lett., **56** (1986) 2533.
34. L.C. Andreani, F. Tassone, F. Bassani, Solid State Comm., **77** (1991) 641
35. D.S. Citrin, Phys. Rev. **B47** (1993) 3832.
36. A. Ourmazd, D.W. Taylor, J. Cunningham, C.W. Tu, Phys. Rev. Lett., **62** (1989) 933.
37. D. Gammon, B.V. Shanabrook, D.S. Katzer, Phys. Rev. Lett., **67** (1991) 1547.
38. N.W. Ashcroft, N.D. Mermin: *Solid State Physics*, Holt, Rinehart and Winston, New York, 1976.
39. H. Haug, S.W. Koch: *Quantum theory of the optical and electronic properties of semiconductors*, World Scientific, Singapore (1990).
40. W.W. Chow, S.W. Koch: *Semiconductor-Laser Physics*, Springer Verlag, Berlin (1994).
41. G.D. Mahan: *Many Particle Physics*, Plenum Press, New York (1981).
42. A.C. Gossard, A. Pinczuk: *Synthetic Modulated Structures*, ed., by L.L. Chang, B.C. Giessen (Academic Press, New York 1985) 215.
43. W. Kohn, L.J. Sham, Phys. Rev. **A140** (1965) 1133.
44. M. Bugajski, S. Łepkowski, Electron Technology, **30**, no.4 (1997) to be published.
45. A.E. Ruckenstein, S. Schmitt-Rink, Phys. Rev. **B35** (1987) 7551.
46. M.S. Skolnick, J.M. Rorison, K.J. Nash, D.J. Mowbray, P.R. Tapster, S.J. Bass, A.D. Pitt, Phys. Rev. Lett. **58** (1987) 2130.
47. Y.H. Zhang, N.N. Ledentsov, K. Plog, Phys. Rev. **B44** (1991) 1399.
48. G.D. Mahan, Phys. Rev. **153** (1967) 882.
49. S. Haacke, R. Zimmermann, D. Bimberg, H. Kal, D.E. Mars, J.N. Miller, Phys. Rev. **B45** (1992) 1736.
50. J.F. Mueller, Phys. Rev. B42, **11** (1990) 189.